Electronic Supplementary Material (ESI) for Sustainable Energy & Fuels.

Porous Carbon Layers Wrapped Co_3Fe_7 Alloy Derived from a Bimetallic Conjugated Microporous Polymer as Trifunctional Electrocatalyst for Rechargeable Zn-air Battery and Self-powered Overall Water Splitting

Wenxue Guo,[†a] Xiujuan Luan,[†a] Peng Sun,[†a] Tao Wang,[†c] Hantian Luo,[a] Xiaotong Li,[b] Chengde Li,*[a] Wei Tan,*[b] Jingkun Bai,*[e] Qiang Wang,*[d] Baolong Zhou*[a,b]

[a.] *School of Pharmacy, Weifang Medical University, Weifang, 261053, Shandong, P. R. China.*

[b.] *Department of Respiration, The First Affiliated Hospital of Weifang Medical University (Weifang People's Hospital), Weifang, 261031, Shandong, P.R. China.*

[c.] *Department of Cardiology, Affiliated Hospital of Weifang Medical University, Weifang, Shandong, P. R. China.*

[d.] *Department of Epidemiology, Weifang Medical University, Weifang, 261053, Shandong, China.*

[e.] *School of Bioscience and Technology, Weifang Medical University, Weifang, 261053, PR China*

E-mail: zhoubaolong@wfmc.edu.cn

†These authors contribute equally to this article.

Contents

Section 1. Materials and Methods

Low temperature N_2 adsorption-desorption measurements were conducted *via* a Bel Japan Inc. Model BELSOPR-mini II analyser. All samples were initially degassed at 300 ^oC for 5 h under a high vacuum of 10^{-5} bar before analysis to remove the solvent absorbed in the porous skeleton. Pore size distributions curves (PSDs) were obtained from the adsorption isotherms by the NLDFT method. Total pore volumes were calculated from the uptake at a relative pressure of 0.995. The specific surface areas for N_2 were calculated based on the BET model over a relative pressure (P/P_0) between 0 and 1.0. Fourier Transform Infrared Spectroscopy (FTIR) was performed on KBr pellets in the range of 4000 to 500 cm^{-1} using Spectrum Spotlingt 400. The element content was tested using ICP to and element analysis. Inductively Coupled Plasma OES spectrometer (ICP) was conducted on Ultima 2 produced in HORIBA Jobin Yvon. Elemental analyses (C, H, and N) were performed on an Elementar Vario MICRO elemental analyzer. Powder X-ray diffraction (PXRD) parameters were obtained using a Rigaku-DMAX 2500 diffractometer at a rate of 5^o min^{-1} from 10^o to 80^o. Scanning electron microscopy (SEM) were carried out on a JEM-1230, JEOL, Tokyo, Japan at 10.0 kV. Transmission electron microscopies (TEM) were conducted on a FEI model Tecani 20 microscope and a JEOL model JSM-2100F. The samples used in the SEM and TEM were fabricated by drop-casting a super sonicated ethanol suspension of target samples (polymers and catalysts) onto a copper grid. The chemical composition of the as-synthesized monomer was analyzed by the ^1H NMR spectrometer (avance-500 MHZ NMR of Bruker company, Switzerland), mainly using deuterium chloroform and deuterium DMSO as solvent.

Thermogravimetry (TGA) of prepared polymer samples was carried out in a TGA Instruments thermal analyzer TA-SDT Q-600. Raman spectrum was examined on a LabRAM HR at the range from the 500 to 3500 cm^{-1}. X-ray Photoelectron Spectroscopy (XPS) was conducted on XPSESCALAB 250Xi analyser. Solid state ^{1}H-^{13}C NMR spectra is mainly tested through the AVANCE III 400 MHz spectroscopic light of BRUKER. The sample was tested at a scan frequency of 10 kHz.

Section 2. Synthetic Procedures

Materials

Unless noted, all the chemicals are purchased from commercial suppliers and used directly without further purification. Ferrocene, n-butyllithium solution, and *N*,*N*,*N*,*N*-tetramethylethylethylenediamine (TMEDA) were received from Aladdin, China. Cobaltous chloride ($CoCl_2$) were purchased from Energy Chemical, China. N, N-Dimethylformamide was purchased from Xilong Scientific. *N, N*-Dimethylformamide and pyrrole was treated redistilled under reduced pressure. The remaining active 4 Å molecular sieves are sealed and stored in a desiccator for later use. Glacial acetic acid and else organic solvents were provided from the commercial source used directly without further purification.

Synthesis of Ferrocenediformaldehyde.

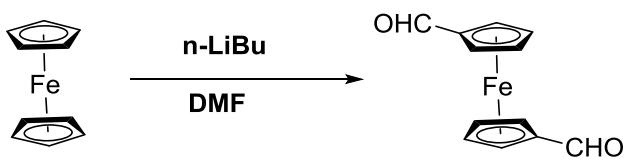

Scheme S1. Route for the synthesis of Ferrocenediformaldehyde.

The reaction was carried out under anhydrous and anaerobic conditions. To a solution of Ferrocene (10 g, 54 mmol) in hexane (100 mL) was sequentially added n-butyllithium solution (120 mL) and TMEDA (17 mL, 56 mmol). The reaction mixture was stirred for 20 hours at room temperature. Then, DMF (13 mL) was slowly dropped into the solution at -78 °C. Then the reaction was natural warmed to room temperature and reacted for 4 h. After that, hydrochloric acid (4.0 M, 0.2 mol) was added to quench the reaction. Subsequently, 200 mL H_2O was added and extract with 3 × 200 mL of $CHCl_3$. The organic phase was collected and dried with $MgSO_4$. Then it was evaporated to dry to get the product. The crude mixture was purified by column chromatography (Petroleum ether: ethyl acetate 3:1-4:1) providing a bright red diamond crystal. Yield: 3.8 g, 51%.[1] ^{1}H NMR in (300 MHz, CDCl3) δ: 4.68 (s, 4H, C_5H_4); 4.89 (s, 4H, C_5H_4); 9.95 (s, 2H, -CHO).

Synthesis of Fc-Por.

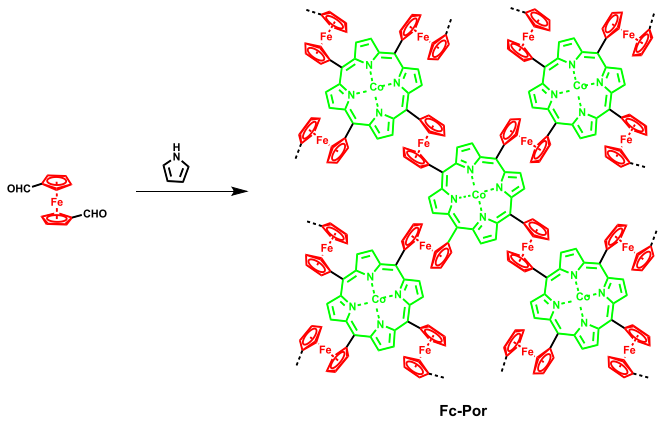

Scheme S2. Route for the synthesis of Fc-Por.

In a typical experimental procedure[2], a flame dried round bottom flask was charged with freshly distilled pyrrole (0.05 g, 0.74 mmol) and 1,1'-ferrocene-dicarboxaldehyde (0.18 g 0.74 mmol). Then 15 mL glacial acetic acid was taken in the flask with constant stirring along with cobaltous chloride (1.2 equivalent) under inert Argon atmosphere. The whole solution was stirred at 300 rpm to make the whole solution homogenized. After 6 h, the mixture was transferred to a Teflon lined autoclave and kept under hydrothermal treatment for 72 h at 180

°C. Then, the oven was slowly cooled to room temperature, resulting a dark brownish product which separates out from the mixture. The precipitates were filtered and thoroughly washed with distilled water, methanol, acetone, THF, dichloromethane and then vacuum dried in an oven at 80 °C for another 48 h. The material was then rigorously washed by Soxhlet extractions for 24 h with water, dichloromethane, methanol, and tetrahydrofuran (THF), respectively, to give Fe-POP as a black powder (0.2 g).

Synthesis of FP-X:

FP-X was prepared via direct carbonization of Fc-Por under the Ar. Briefly, after fine grinding, Fc-Por was loaded on a porcelain boat and then transferred into a tube furnace. Then, the pyrolysis was conducted under the atmosphere of Ar and heated to the target temperature (X =850, 950 and 1050 °C) for 2 h.

Section 3: Electrochemical Measurements[3,4]

All electrochemical tests were examined via a standard three-compartment cell at room temperature. According to the Nernst equation, $E_{(RHE)} = E_{(Ag/AgCl)} + 0.059 \times pH + 0.197$ V, at 25 °C), the total potentials were referenced to the reversible hydrogen electrode (RHE). Apart from a rotating disc electrode (RDE) composed of a glassy carbon disc (4.0 mm diameter), a rotating ring disc electrode (RRDE) was constructed by a glassy carbon disc (4 mm diameter) surrounded by an outer Pt-ring (with an inner-diameter of 5 mm and outer-diameter of 7 mm), which played role in working electrodes. The catalyst inks were loading on the surface of work electrode. The catalyst inks were fabricated by dispersing 5 mg Catalyst into the mixture of 25 μL Naffion, 100 μL H_2O and 375 μL ethanol under an ultrasonic bath for 1 hour to get even suspensions. 8 μL catalyst link was pipetted onto the glassy carbon surface of the RDE or the

RRDE and leave it to dry in air at room temperature.

The catalytic activities toward ORR of prepared samples were estimated by CV, RRDE and RDE measurements technique via a three-electrode cell system on a CHI-760E electrochemical workstation (CH Instruments). All the experiments were carried out in either alkaline conditions (0.1 M KOH) or neutral media (0.1 M PBS) saturated with O_2 or Ar. The CV measurements and the RDE/RRDE experiments were examined with a scan rate of 5 mV s^{-1} at the potential between − 0.8 V and + 0.3 V with different rotating speeds from 400 to 2500 rpm. According to K-L equations measured by Koutecky-Levich (K-L) plots in different electrode potentials, the electron transfer numbers (n) were computed by the slopes about their best linear fit lines. [6,7]

$$\frac{1}{J} = \frac{1}{J_L} + \frac{1}{J_K} = \frac{1}{BW^{1/2}} + \frac{1}{J_K} \qquad (1)$$

In the equation, J_L is the measured current; J_K represents the kinetic-limiting current and w is the rotation speeds of electrode.

$$B = 0.62nFC_0(D_0)^{2/3}V^{-1/6} \qquad (2)$$

In equation 2, n is the number of transferred electrons during ORR; *F* is Faradaic constant (F = 96485 C mol^{-1}), C_0 is the O2 concentration (solubility) in 0.1 M KOH electrolyte (1.2×10^{-6} mol cm^{-3}); D_0 is the O_2 diffusion coefficient (1.90×10^{-5} cm^2 s^{-1}) and V is the kinematic viscosity of the O_2 saturated 0.1 M KOH solution (0.01 cm^2 s^{-1}).

For the RRDE measurements, the peroxide percentage (H_2O_2 yields) and the transferred number of electron (n) were calculated according to the following equations 3 and 4. [8]

$$H_2O_2\% = 200 \times \frac{I_r/N}{I_d + I_r/N} \qquad (3)$$

$$N = 4 \times \frac{I_d}{I_d + \frac{I_r}{N}} \qquad (4)$$

In equation 3 and 4, Id is the disk current, and Ir refers to the ring current and N represents

the current collection efficiency of the Pt ring.

H_2 or O_2 production rate (mol h^{-1}) is calculated according to the following equation.

$$\text{Gas production rate} = \frac{V/V_M}{t} \qquad (5)$$

In equation 5, V (L) is the gas volume, t (h) is the test time, V_M is the molar volume of gas (24.5 L mol^{-1} at 25 ^oC, 101 kPa).

Section 4. PXRD Profile

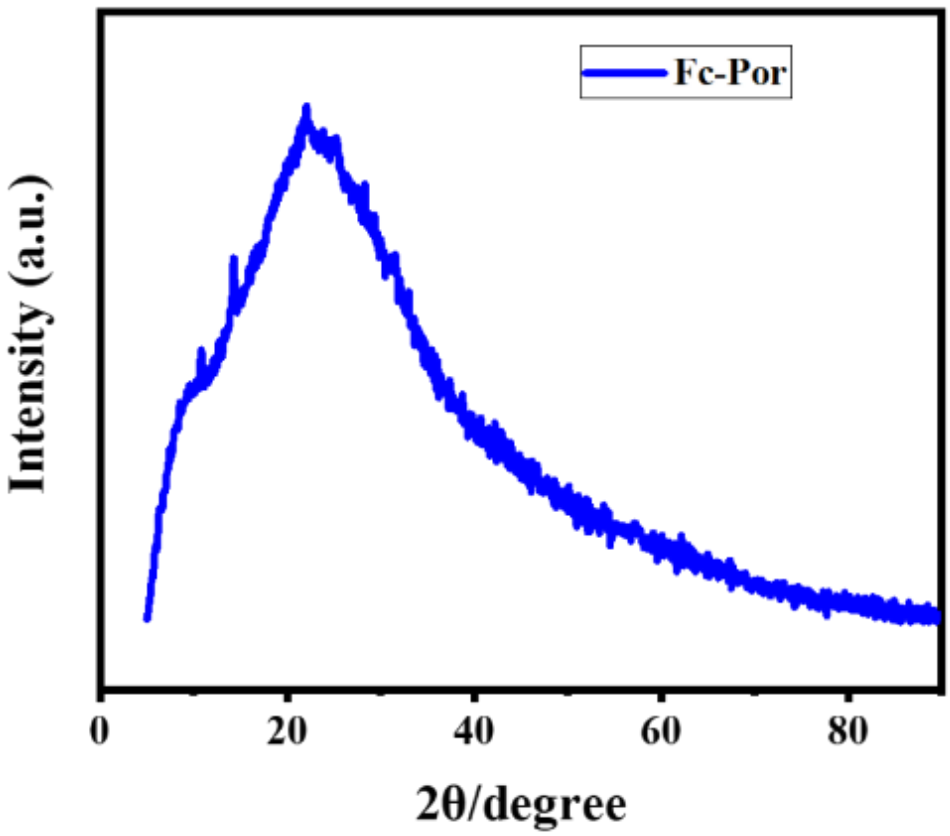

Figure S1. Powder XRD of Fc-Por.

Section 5. TGA

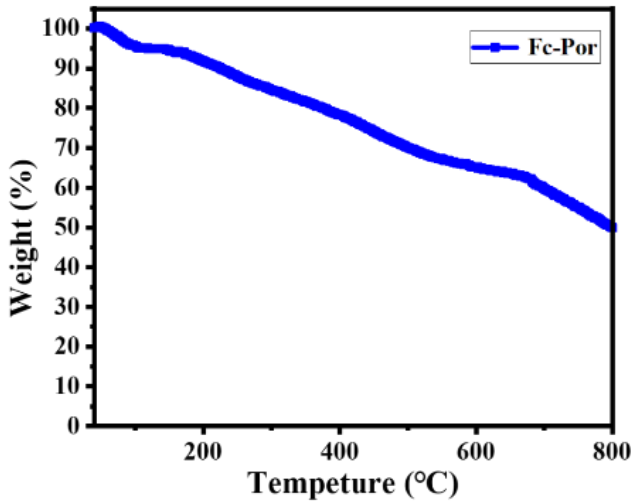

Figure S2. TGA of Fc-Por.

Section 6. PSD curves based on the BJH model

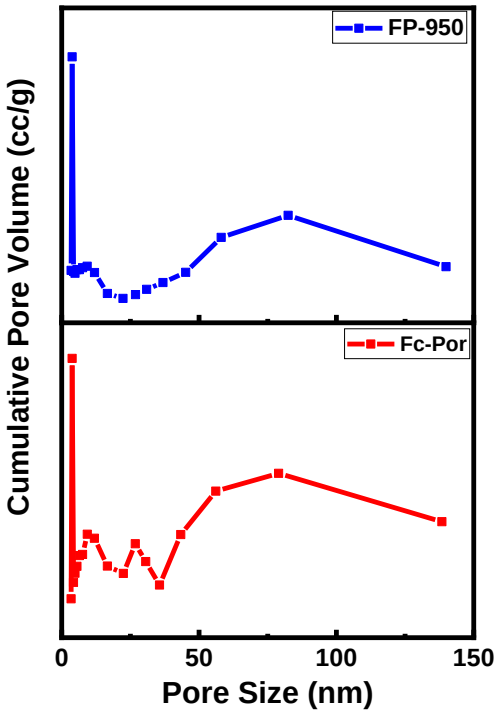

Figure S3. PSD curves based on the BJH model.

Section 7. TEM

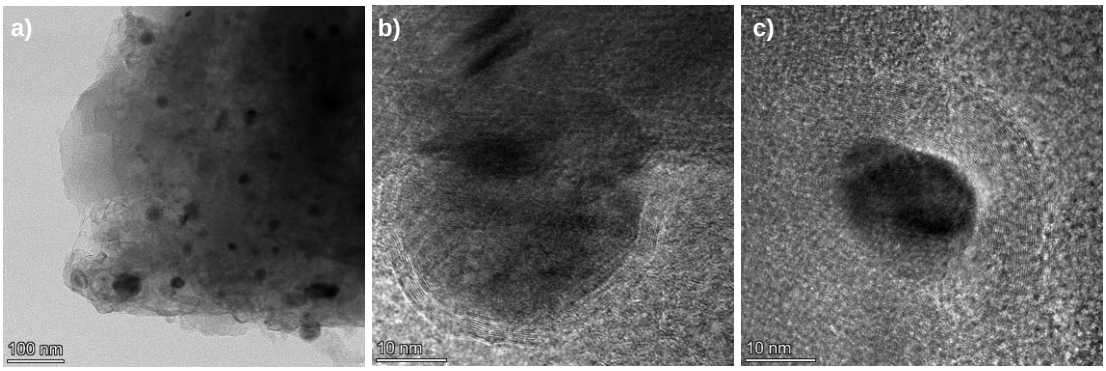

Figure S4. TEM of FP-950.

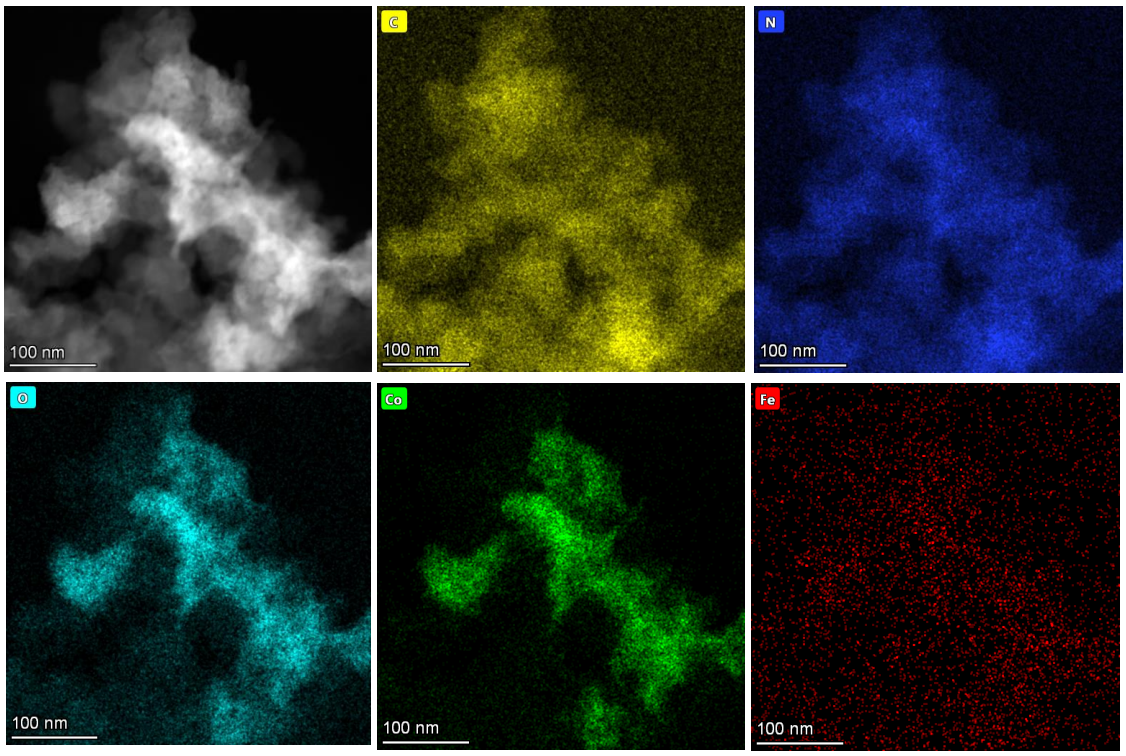

Figure S5. Elemental mapping of FP-850 after acid etching.

Section 8. X-ray Photoelectron Spectra (XPS)

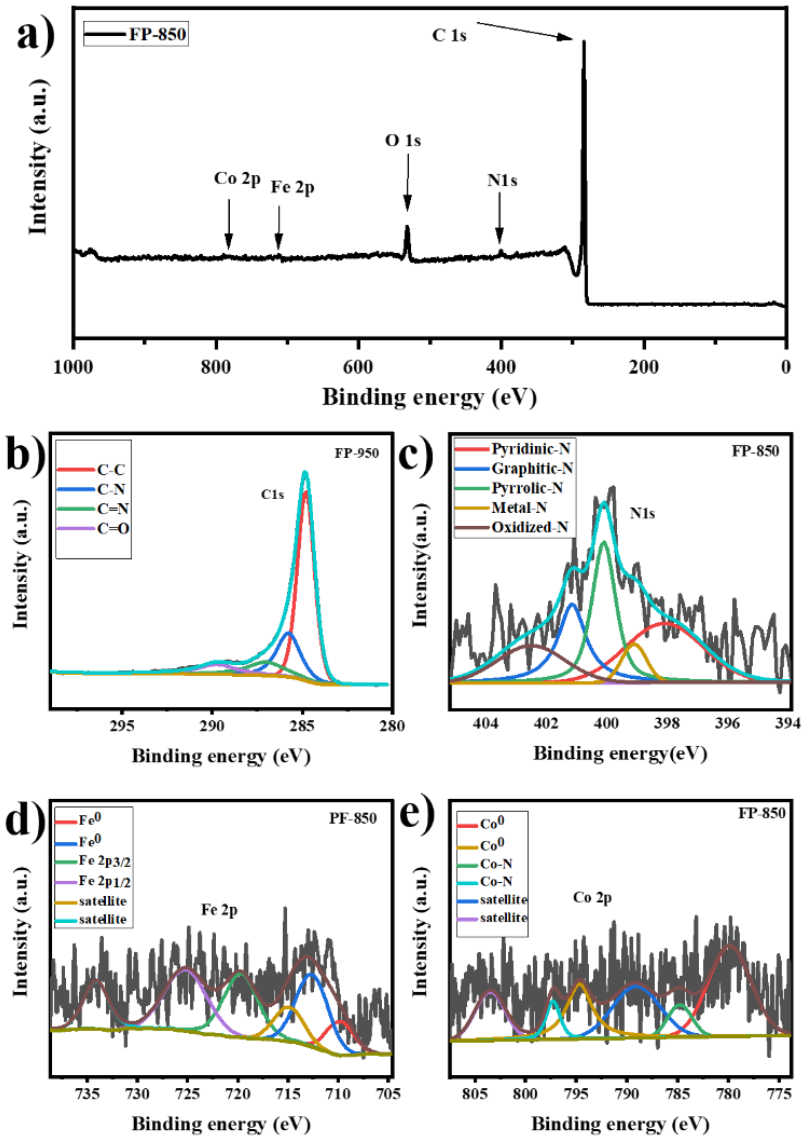

Figure S6. a) XPS survey full scan of FP-850; b) High-resolution C 1s spectra of FP-850; c) High-resolution N 1s spectra of FP-850; d) High-resolution Fe 2p spectra of FP-850; e) High-resolution Co 2p spectra of FP-850.

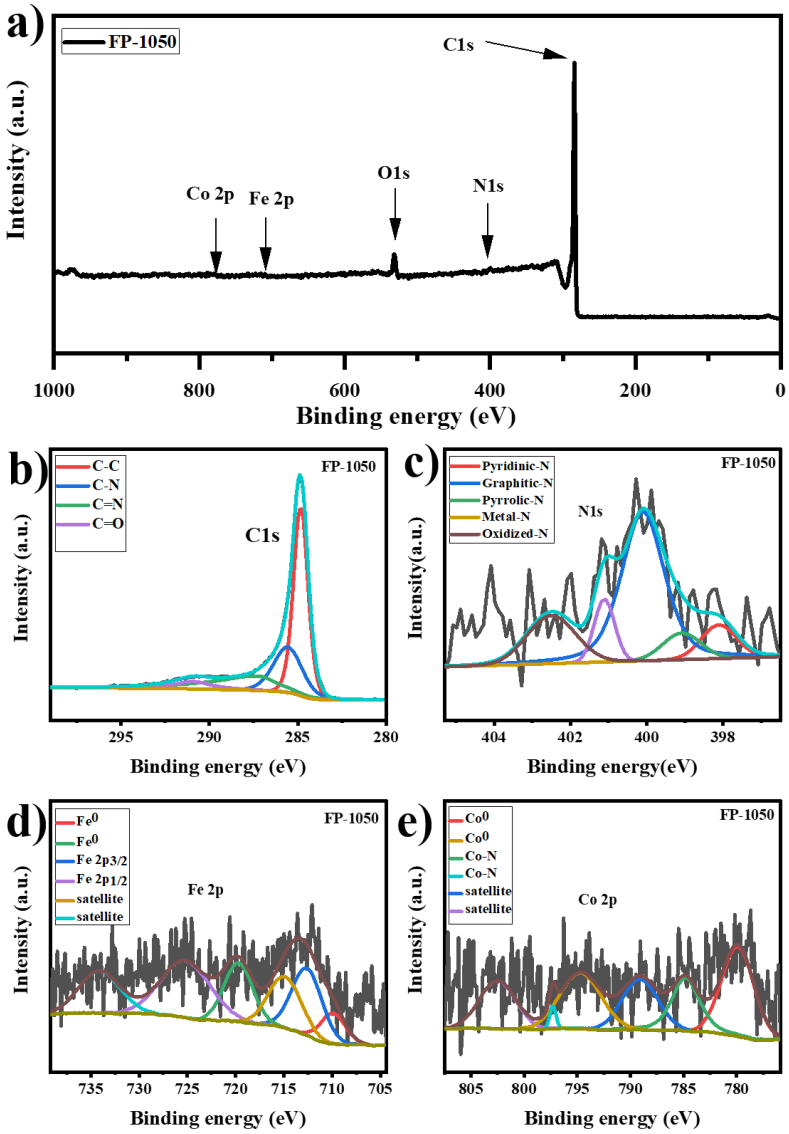

Figure S7. a) XPS survey full scan of FP-1050; b) High-resolution C 1s spectra of FP-1050; c) High-resolution N 1s spectra of FP-1050; d) High-resolution Fe 2p spectra of FP-1050; e) High-resolution Co 2p spectra of FP-1050.

Section 9. Electrochemical Performance

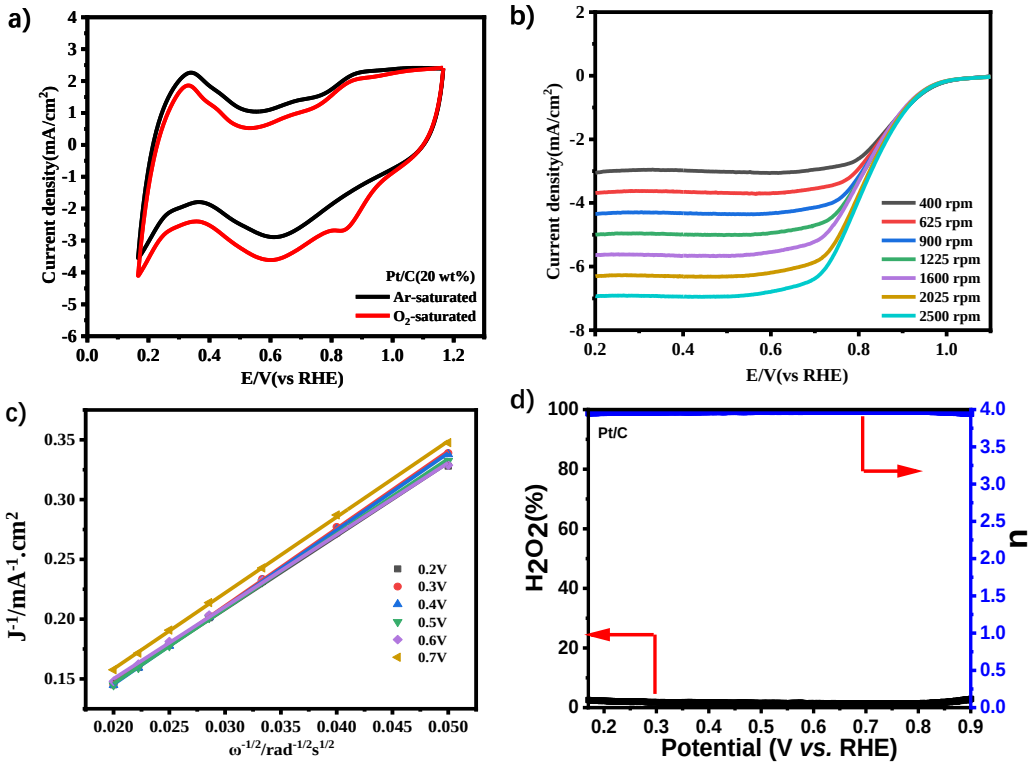

Figure S8. a) CV curves of commercial Pt/C (20%) on a glassy carbon electrodes in 0.1 M KOH saturated with O_2 or Ar at a sweep rate of 50 mV s^{-1}; b) LSV of commercial Pt/C (20%) at various rotation speeds; c) K-L plots curves of commercial Pt/C (20%); d) Percentage of hydrogen peroxide yield and the electron transfer number (n) of Pt/C at different potentials.

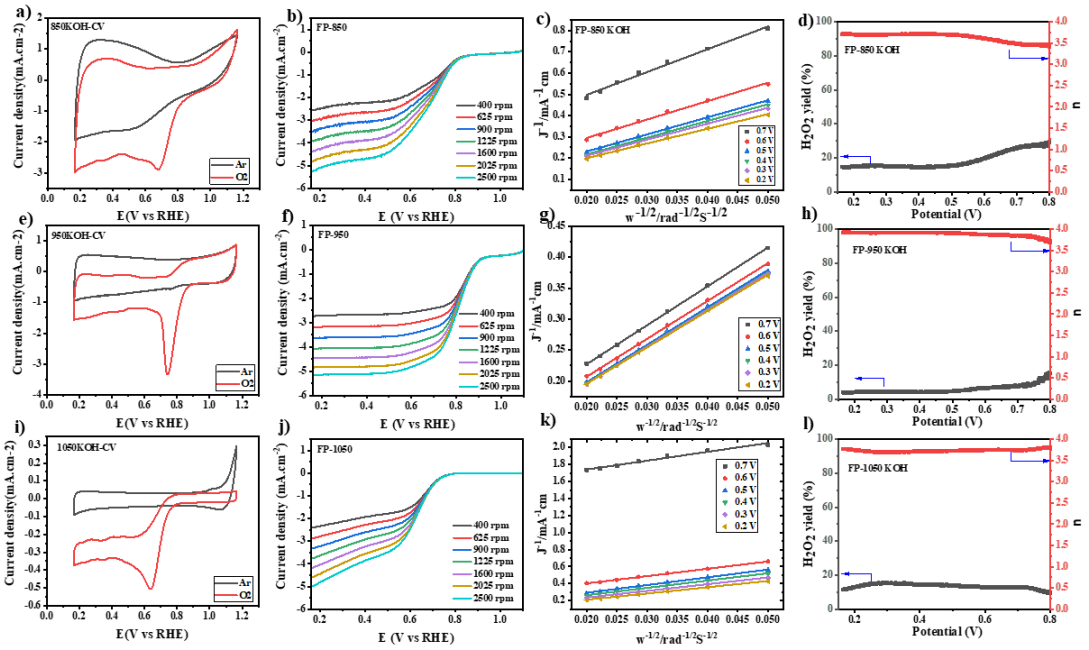

Figure S9. Electrochemical performance of as-prepared contrast catalysts in water solution of 0.1 M KOH. a) CV curves of PF-850; b) LSV of PF-850 at different rotation speeds; c) K-L plots of PF-850; d) Percentage of hydrogen peroxide yield and the electron transfer number (n) of PF-850 at different potentials; e) CV curves of FP-950; f) LSV of FP-950 at different rotation speeds; g) K-L plots of FP-950; h) Percentage of hydrogen peroxide yield and the electron transfer number (n) of FP-950 at different potentials; i) CV curves of PF-1050; j) LSV of PF-1050 at different rotation speeds; k) K-L plots of PF-1050; l) Percentage of hydrogen peroxide yield and the electron transfer number (n) of PF-1050 at different potentials.

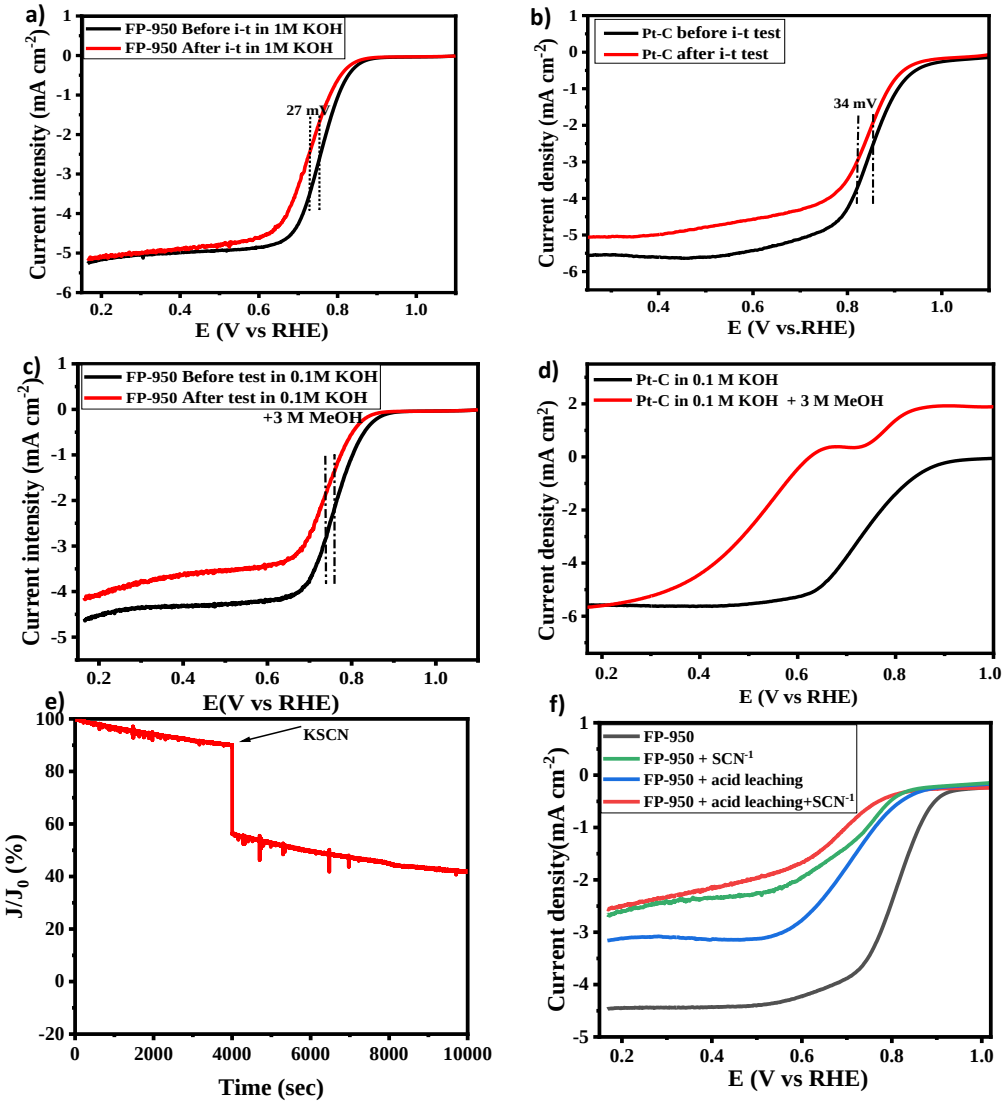

Figure S10. a) Polarization curves of FP-950 measured by RDE in O_2-saturated 0.1 M KOH before (red line) and after (black line) the i-t (20000 s) experiments; b) Polarization curves of Pt/C (20%) measured by RDE in O_2-saturated 0.1 M KOH before (red line) and after (black line) the i-t (20000 s) experiments; c) LSV curve of FP-950 measured before and after the injection of 3 M methanol; d) LSV curve of Pt/C measured before and after the injection of 3 M methanol; e) I-t response towards the addition of SCN^{-1} and the insert part is corresponding LSV curve collected before/after the i-t tests; f) LSV curves recorded before/after the acid treatment.

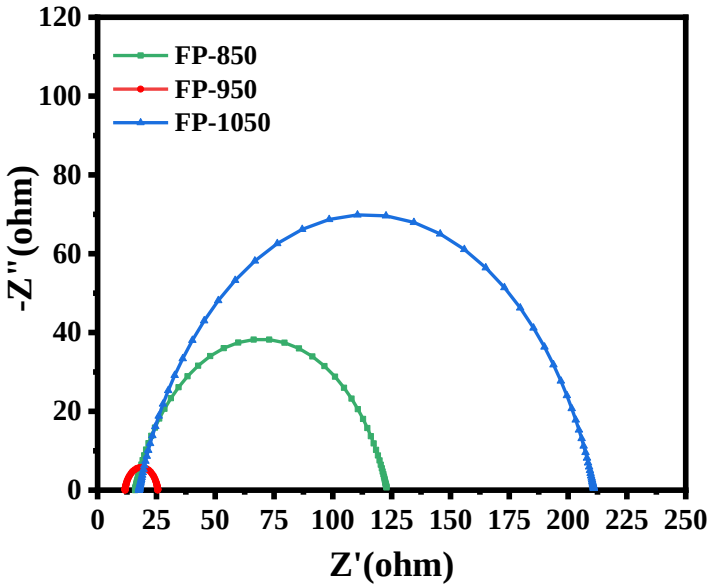

Figure S11. Electrochemical impedance spectroscopy (EIS) of FP-X catalysts towards OER in 1 M KOH.

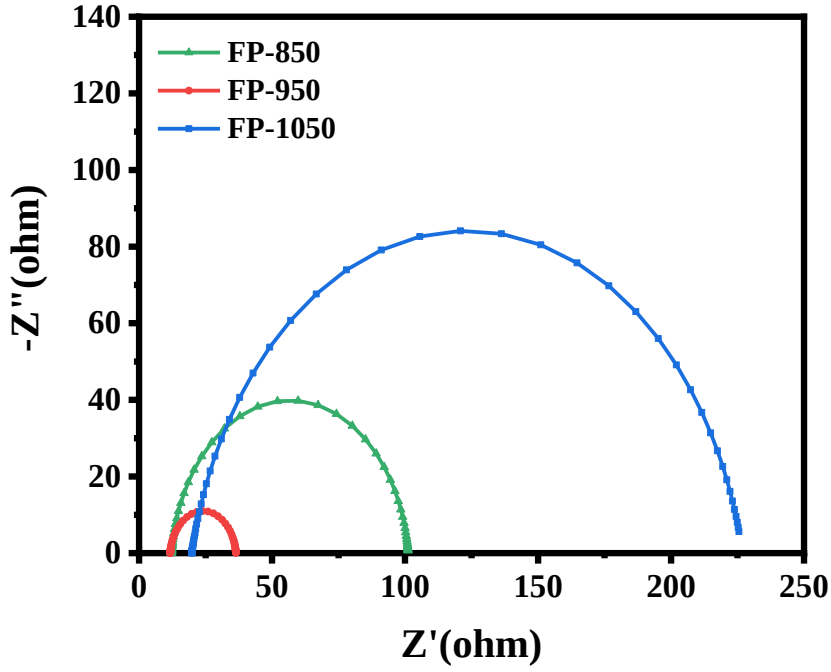

Figure S12. Electrochemical impedance spectroscopy (EIS) of FP-X catalysts towards HER in 1 M KOH.

Section 10. TEM of catalyst after Zn-air battery test

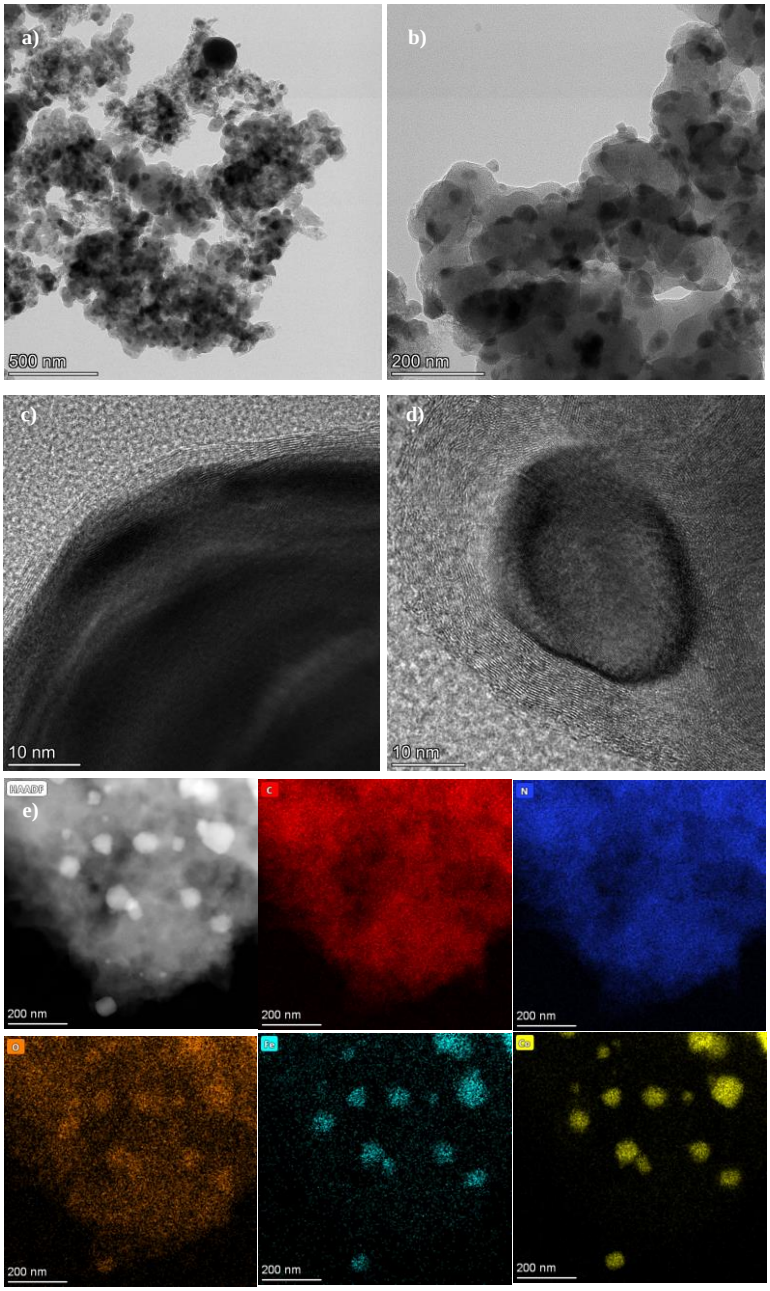

Figure S13. TEM of FP-950 which has underwent the long time charge-discharge running for Zn-air battery

Section 11. XPS after Zn-air battery test

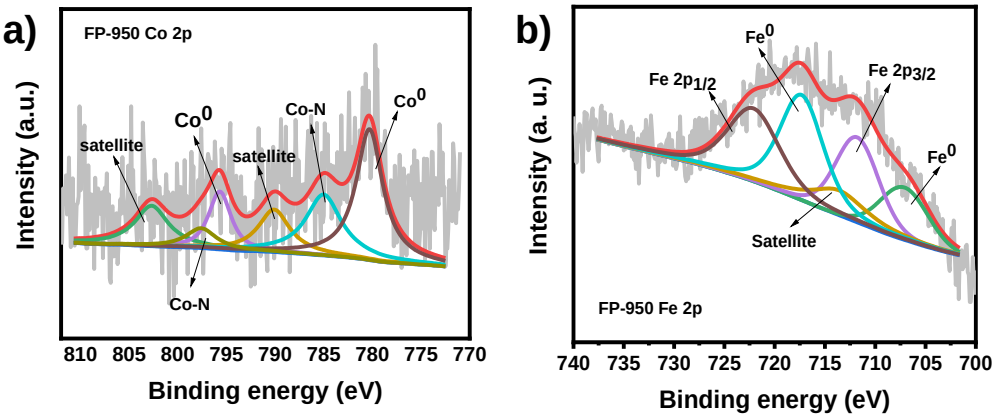

Figure S14. XPS on FP-950 which has underwent the long time charge-discharge running for Zn-air battery a) High-resolution Co 2p spectra of FP-950. b)High-resolution Fe 2p spectra of FP-950

Section 12. Supporting Tables

Table S1. Porosity parameters of prepared polymers and corresponding catalysts

Sample	S_{BET} (m^2/g)	V_{Total} (m^3/g)	Pore width distribution (nm)
Fc-Por	127.8	0.105	1.03/1.46/2.10/3.93
FP-950	520.4	0.28	0.66/1.57/2.63

Table S2. The surface element contents of different species including carbon, oxygen, nitrogen and iron in as-synthesized catalysts, calculated from the XPS spectra

Sample	C (%)	N (%)	O (%)	Fe (%)	Co (%)
FP-850	89.58	2.78	6.63	0.39	0.62
FP-950	89.39	5.74	4.33	0.38	0.16
FP-1050	93.25	1.32	4.57	0.68	0.18

Table S3. The surface contents of different N species in PF-X catalysts, calculated from the XPS spectra

Sample	Pyridinc-N in total N (%) vs total element (wt%)	Metal-N in total N (%) vs total element (wt%)	Pyrrolic-N in total N (%) vs total element (wt%)	Graphitic-N in total N (%) vs total element (wt%)	Oxidized-N in total N (%) vs total element (wt%)
FP-850	29.25 (0.81)	6.14 (0.17)	27.35 (0.76)	21.07 (0.59)	16.19 (0.45)
FP-950	9.53 (0.55)	20.64 (1.18)	32.14 (1.84)	20.37 (1.17)	17.31 (0.99)
FP-1050	8.91 (0.12)	7.57 (0.10)	56.32 (0.74)	9.66 (0.13)	17.54 (0.23)

Table S4. Main parameters of the prepared catalysts combined with the commercial Pt/C in alkaline conditions

Sample	E_{Onset} (E_{onset}, V)	$E_{1/2}$ ($E_{1/2}$, V)	Electron transfer number (n, at 0.5 V)	Current density (mA cm^{-2} at 0.5V)
FP-850	0.909	0.671	3.691	3.703
FP-950	0.94	0.808	3.909	4.396
FP-1050	0.764	0.612	3.724	2.952
Pt/C (20%)	1.031	0.810	3.970	5.633

Table S5. The comparison of the electrochemical performance toward ORR among different non-noble metal catalysts in 0.1 M KOH.

Catalyst	Electrolyte	E_{Onset} (V vs RHE)	$E_{1/2}$ (V vs. RHE)	Ref.
Co/CoP–HNC	0.1M KOH	0.94	0.83	[3]
PPy/FeTCPP/Co	0.1M KOH	1.01	0.86	[4]
NCF-900	0.1M KOH	1.05	0.89	[5]
FePx/Fe-N-C/NPC	0.1M KOH	1.01	0.86	[6]
Ni-NC700	0.1M KOH	0.86	0.75	[7]
CoNx/NGA	0.1M KOH	0.93	0.83	[8]
CoOx/CoNy@CNz,700	0.1M KOH	0.9	0.83	[9]
W_2N/WC	0.1M KOH	0.93	0.81	[10]
Co_2P/NPG-900	0.1M KOH	0.94	0.81	[11]
N/CF-EC-900	0.1M KOH	0.984	0.849	[12]
FP-950	0.1M KOH	1.09	0.808	This work

Table S6. The comparison of the electrochemical performance toward OER and HER among other trifunctional electrocatalysts catalysts in 1M KOH.

Catalyst	Electrolyte	OER Overpotential at j=10 mA/cm^2	HER Overpotential at j=10 mA/cm^2	Ref.
Co/CoP-HNC	1M KOH	0.3	0.18	[3]
CoPNCs	1M KOH	0.28	0.0625	[14]
FeS/Fe3C@N‐S‐C‐800	1M KOH	0.57	0.45	[15]
FeCo/NPC	1M KOH	0.36	0.33	[16]
PPy/FeTCPP/Co	1M KOH	0.34	0.27	[17]
Co@N-CNTF-2	1M KOH	0.35	0.26	[18]
Fe_3C‐Co/NC	1M KOH	0.34	0.238	[19]
FP-950	1M KOH	0.346	0.304	This work

Table S7. Comparison of zinc-air battery utilizing FP-950 with other noble-metal free electrocatalysts reported recently.

Catalysts	Loading ($mg\ cm^{-2}$)	Open circuit Voltage (V)	Peak power ($mW\ cm^{-2}$)	Reference
Fe/Fe_2O_3@Fe-N-C	2	1.47	220	[20]
NC@Co–NGC DSNCs	0.5	1.45	108	[21]
CNF@Zn/CoNC	0.5	1.46	140.1	[22]
NCo@CNT-NF700	0.5	1.46	220	[23]
Co/CoxSy@SNCF-800	2	1.37	230	[24]
FeNiP/NCH	1	1.48	250	[25]
NiSx/NMC-1.5	1	1.53	186	[26]
BHPC-950	0.5	1.44	197	[27]
Fe/OES	0.52	1.51	186.8	[28]
PB@Met-700	2	1.41	148	[29]
FP-950	1	1.41	167.4	This work

Table S8. The comparison of the electrochemical performance toward ORR, OER and HER among different non-noble metal catalysts

Catalyst	ORR $E_{1/2}$ (V vs. RHE)	OER Overpotential at j=10 mA/cm^2	HER Overpotential at j=10 mA/cm^2	Ref.
Co_9S_8@Co_9S_8@MoS_2 -0.5	0.776 V	1.57 V	-0.173 V	[30]
Ca_2FeRuO_6	0.9 V	1.57 V	-0.19 V	[31]
NiSAs@ACNTFs	0.86 V	1.48 V	-0.49 V	[32]
$Sr_{0.95}Nb_{0.1}Co_{0.9-x}Ni_xO_{3-\delta}$	0.87 V	1.5 V	-0.229 V	[33]
NCN-1000-5	0.78 V	1.55 V	-0.09 V	[34]
$CoNiO_2$/SNC	0.7 V	1.56 V	-0.43 V	[35]
Co@N-CNTF-2	0.91 V	1.58 V	-0.266 V	[36]
FP-950	0.808	1.57 V	-0.304 V	This Work

Section 13. Supporting References

[1] G.G.A. Balavoine, G. Doisneau, T. Fillebeen-Khan, *J. Organomet. Chem.*, 1991, **412**, 381-382.

[2] A. Modak, M. Nandi, J. Mondal, A. Bhaumik, *Chem. Commun.*, **2012**, *48*, 248-250.

[3] Y. Hao, Y. Xu, W. Liu, X. Sun, *Mater. Horiz.*, 2018, **5**, 108-115.

[4] X. Zhu, T. Jin, C. Tian, C. Lu, X. Liu, M. Zeng, X. Zhuang, S. Yang, L. He, H. Liu, S. Dai, *Adv. Mater.*, 2017, **29**, 1704091.

[5] X. Yang, K. Li, D. Cheng, W.L. Pang, J. Lv, X. Chen, H.Y. Zang, X.L. Wu, H.Q. Tan, Y.H. Wang, Y.G. Li, *J. Mater. Chem. A*, 2018, **6**, 7762-7769.

[6] Q. Qin, H. Jang, P. Li, B. Yuan, X. Liu, J. Cho, *Adv. Energy Mater.*, 2019, **9**. 1803312

[7] B. Devi, R.R. Koner, A. Halder, *ACS Sustain. Chem. Eng.*, 2019, **7**, 2187-2199.

[8] H. Zou, G. Li, L. Duan, Z. Kou, J. Wang, *Appl Catal B-Environ.*, 2019, **259**, 118100.

[9] J. Liu, C. Wang, H. Sun, H. Wang, F. Rong, L. He, Y. Lou, S. Zhang, Z. Zhang, M. Du, *Appl Catal B-Environ.*, 2020, **279**, 119407.

[10] J. Diao, Y. Qiu, S. Liu, W. Wang, K. Chen, H. Li, W. Yuan, Y. Qu, X. Guo, *Adv. Mater.*, 2020, **32**, 1905679.

[11] Q. Shao, Y. Li, X. Cui, T. Li, H. Wang, Y. Li, Q. Duan, Z. Si, *ACS Sustain. Chem. Eng.*, 2020, **8**, 6422.

[12] S.M. Alshehri, A.N. Alhabarah, J. Ahmed, M. Naushad, T. Ahamad, *J Colloid Interf. Sci.*, 2018, **514**, 1-9.

[13] J. Bai, T. Meng, D. Guo, S. Wang, B. Mao, M. Cao, *ACS Appl. Mater. Inters.*, 2018, **10**, 1678.

[14] H. Li, Q. Li, P. Wen, T.B. Williams, S. Adhikari, C. Dun, C. Lu, D. Itanze, L. Jiang, D.L. Carroll, G.L. Donati, P.M. Lundin, Y. Qiu and S.M. Geyer, *Adv. Mater.*, 2018, **30**, 1705796.

[15] F. Kong, X. Fan, A. Kong, Z. Zhou, X. Zhang, Y. Shan, *Adv. Funct. Mater.*, 2018, **28**, 1803973.

[16] H.X. Zhong, J. Wang, Q. Zhang, F. Meng, D. Bao, T. Liu, X.Y. Yang, Z.W. Chang, J.M. Yan, X.B. Zhang, *Adv. Sustain. Syst.*, 2017, **1**,1700020.

[17] J. Yang, X. Wang, B. Li, L. Ma, L. Shi, Y. Xiong, H. Xu, *Adv. Funct. Mater.*, 2017, **27**.1606497.

[18] H. Guo, Q. Feng, J. Zhu, J. Xu, Q. Li, S. Liu, K. Xu, C. Zhang, T. Liu, *J. Mater. Chem. A*, 2019, **7**, 3664-3672.

[19] C.C. Yang, S.F. Zai, Y.T. Zhou, L. Du, Q. Jiang, *Adv. Funct. Mater.*, 2019, **29**, 1901949.

[20] Y. Zang, H. Zhang , X. Zhang, R. Liu, S. Liu, G. Wang, Y. Zhang, H. Zhao, *Nano Res.*, 2016, **9**, 2123-2137.

[21] S. Liu, Z. Wang, S. Zhou, F. Yu, M. Yu, C. Y. Chiang, W. Zhou, J. Zhao, J. Qiu, *Adv. Mater.*, 2017, **29**, 1700874.

[22] Y. Zhao, Q. Lai, J. Zhu, J. Zhong, Z. Tang, Y. Luo, Y. Liang, *Small*, 2018, **14**, 1704207.

[23] L. Zou, C. C. Hou, Z. Liu, H. Pang, Q. Xu, *J. Am. Chem. Soc.*, 2018, **140**, 15393-15401.

[24] S. Liu, X. Zhang, G. Wang, Y. Zhang, H. Zhang, *ACS Appl. Mater. Inter.*, 2017, **9**, 34269-34278.

[25] Y. S. Wei, M. Zhang, M. Kitta, Z. Liu, S. Horike, Q. Xu, *J. Am. Chem. Soc.*, 2019, **141**, 7906-7916.

[26] K. Wan, J. Luo, X. Zhang, C. Zhou, J. W. Seo, P. Subramanian, J.-w. Yan, J. Fransaer, *J. Mater. Chem. A*, 2019, **7**, 19889-19897.

[27] M. Yang, X. Hu, Z. Fang, L. Sun, Z. Yuan, S. Wang, W. Hong, X. Chen, D. Yu, *Adv. Funct. Mater.*, 2017, **27**, 1701971.

[28] C. C. Hou, L. Zou, L. Sun, K. Zhang, Z. Liu, Y. Li, C. Li, R. Zou, J. Yu, Q. Xu, *Angew. Chem. Int. Edit.*, 2020, **59**, 7384-7389.

[29] Y. Lian, K. Shi, H. Yang, H. Sun, P. Qi, J. Ye, W. Wu, Z. Deng, Y. Peng, *Small*, 2020, **16**, 1907368.

[30] J. Li, G. Li, J. Wang, C. Xue, X. Li, S. Wang, B. Han, M. Yang and L. Li, Inorg. Chem. Front., 2020, **7**, 191

[31] N. Kumar, K. Naveen, M. Kumar, T.C. Nagaiah, R. Sakla, A. Ghosh, V. Siruguri, S. Sadhukhan, S. Kanungo and A.K. Paul, ACS Appl. Energy Mater. 2021, **4**, 1323.

[32] S. Dilpazir, P. Ren, R. Liu, M. Yuan, M. Imran, Z. Liu, Y. Xie, H. Zhao, Y. Yang, X. Wang, C. Streb and G. Zhang, ACS Appl. Mater. Interfaces 2020, **12**, 23017.

[33] Q.A. Islam, R. Majee and S. Bhattacharyya, J. Mater. Chem. A, 2019, **7**, 19453.

[34] H. Jiang, J. Gu, X. Zheng, M. Liu, X. Qiu, L. Wang, W. Li, Z. Chen, X. Ji and J. Li, Energy Environ. Sci., 2019, **12**, 322.

[35] Q. Zhang, W. Han, Z. Xu, Y. Li, L. Chen, Z. Bai, L. Yang and X. Wang, RSC Adv., 2020, **10**, 27788.

[36] H. Guo, Q. Feng, J. Zhu, J. Xu, Q. Li, S. Liu, K. Xu, C. Zhang and T. Liu, J. Mater. Chem. A, 2019, **7**, 3664.